JACS
JOURNAL OF THE AMERICAN CHEMICAL SOCIETY
pubs.acs.org/JACS
Article

Highly Stable Zr(IV)-Based Metal–Organic Frameworks for Chiral Separation in Reversed-Phase Liquid Chromatography

Hong Jiang, Kuiwei Yang, Xiangxiang Zhao, Wenqiang Zhang, Yan Liu,* Jianwen Jiang,* and Yong Cui*

Cite This: https://dx.doi.org/10.1021/jacs.0c11276

ABSTRACT: Separation of racemic mixtures is of great importance and interest in chemistry and pharmacology. Porous materials including metal–organic frameworks (MOFs) have been widely explored as chiral stationary phases (CSPs) in chiral resolution. However, it remains a challenge to develop new CSPs for reversed-phase high-performance liquid chromatography (RP-HPLC), which is the most popular chromatographic mode and accounts for over 90% of all separations. Here we demonstrated for the first time that highly stable Zr-based MOFs can be efficient CSPs for RP-HPLC. By elaborately designing and synthesizing three tetracarboxylate ligands of enantiopure 1,1′-biphenyl-20-crown-6, we prepared three chiral porous Zr(IV)-MOFs with the framework formula $[Zr_6O_4(OH)_8(H_2O)_4(\mathbf{L})_2]$. They share the same **flu** topological structure but channels of different sizes and display excellent tolerance to water, acid, and base. Chiral crown ether moieties are periodically aligned within the framework channels, allowing for stereoselective recognition of guest molecules via supramolecular interactions. Under acidic aqueous eluent conditions, the Zr-MOF-packed HPLC columns provide high resolution, selectivity, and durability for the separation of a variety of model racemates, including unprotected and protected amino acids and N-containing drugs, which are comparable to or even superior to several commercial chiral columns for HPLC separation. DFT calculations suggest that the Zr-MOF provides a confined microenvironment for chiral crown ethers that dictates the separation selectivity.

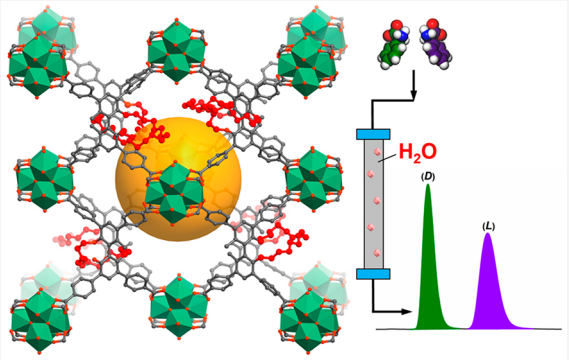

INTRODUCTION

Separation of enantiomers plays a significant role in the pharmaceutical and agrochemical industries, due to the different biological interactions, pharmacology, and toxicity of pure antipodes.[1] This has promoted the enormous development of chiral resolution techniques.[2] Chiral high performance liquid chromatography (HPLC) that relies on the use of chiral stationary phases (CSPs) has proven to be the most popular and efficient method to separate enantiomers.[3] In particular, reversed-phase (RP) HPLC columns are the most popular and account for more than 90% of all HPLC separations.[3a] In RP-HPLC, the mobile phase is water or water-miscible organic mixtures, both of which are safe and easily accessible. Commercial CSPs based on polysaccharide, cyclodextrin, and amino acids show excellent performance in the resolution of a range of racemates, but they lack versatility across all types of chiral analytes and suffer poor stability.[4] So, the exploration of new functional materials as CSPs in chiral chromatography has been a challenging topic for decades. Here we demonstrate, for the first time, that highly stable Zr(IV)-based metal–organic frameworks (MOFs) can serve as efficient CSPs for RP-HPLC in enantiomeric separation.

MOFs have shown potential applications in diverse areas for their permanent porosity and tunable and functionalizable pore structures.[5] MOFs are a priori quite interesting materials as the stationary phase in chromatography, especially liquid chromatography (LC), because their porosity permits high flow rates through it with low back-pressure and, ultimately, favors miniaturization.[6] Consequently, many chiral MOFs have been explored as CSPs for gas and liquid chromatographic enantioseparation.[7,8] However, with few exceptions, these CSPs exhibit unsatisfactory separate factors and resolutions, mainly due to lacking specific interactions between guests and frameworks.[7a,b,8g] Moreover, there are no reports utilizing MOFs as CSPs for RP-HPLC because of their typically limited chemical stability.[6d] Inspiringly, the recent discovery of MOFs made from high-valent metals such as Zr(IV) has greatly increased MOF stability and robustness in water, acid, and base solutions,[9] which are clearly favorable when utilized as CSPs in RP-HPLC. We have recently shown that tetracarboxylate ligands of 1,1′-biphenol can form highly stable and porous Zr-MOFs with a **flu** topology.[10a] We envisaged that

Received: October 26, 2020

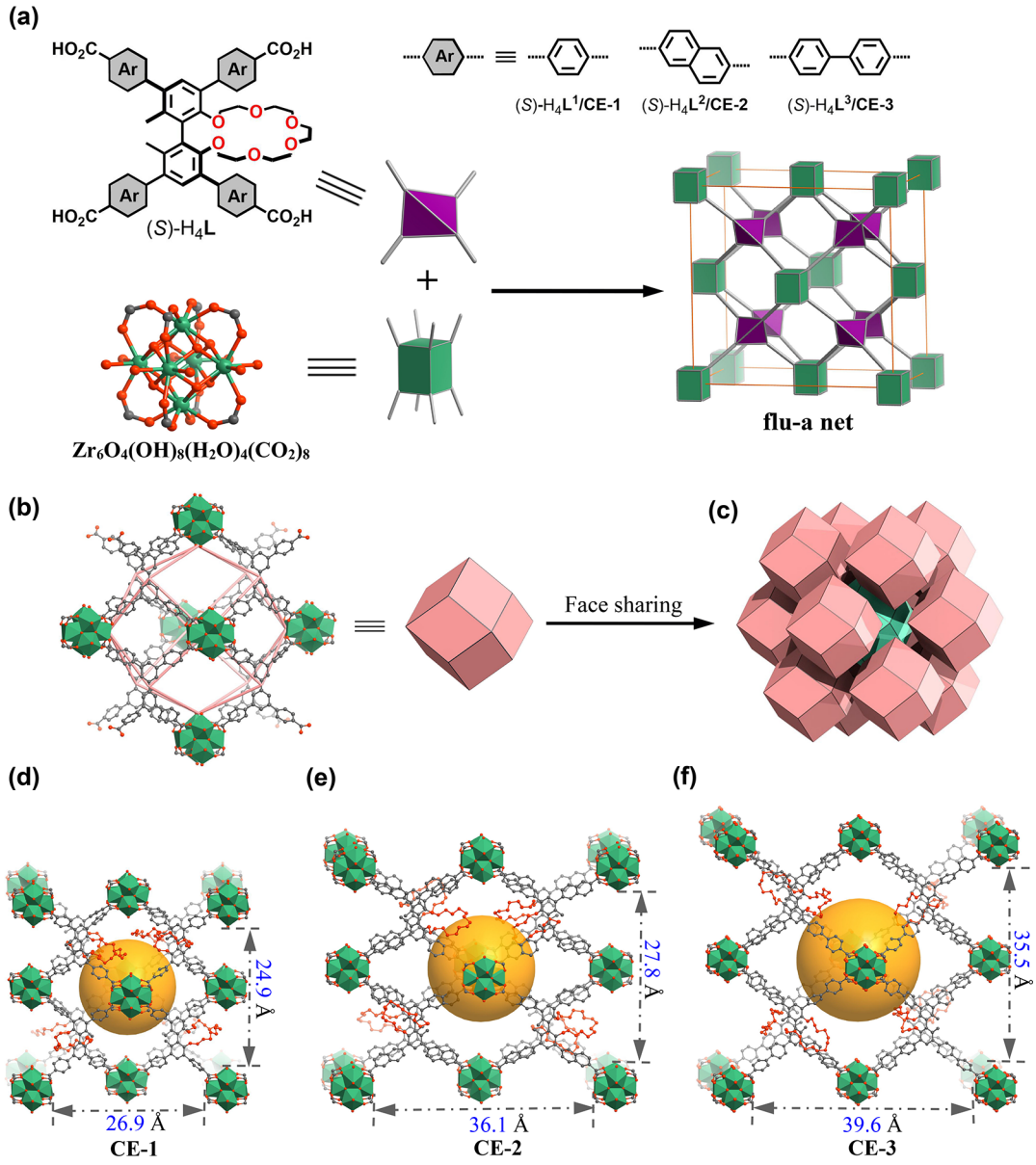

Figure 1. (a) A **flu-a** network constructed by 4-connected linkers and 8-connected Zr nodes. (b) A dodecahedral cage constructed by six Zr_6 clusters and eight ligands (for clarity, methyl, crown ether groups, and H atoms are omitted). (c) Face sharing of the dodecahedra to form the **flu** network. (d–f) View of the three-dimensional structures of **CE-1**, **CE-2**, and **CE-3** (the cavities are highlighted by yellow spheres). The color code is as follows: C, gray; O, red; Zr, green.

incorporating chiral crown ethers into Zr-MOFs may create specific recognition sites with enantioselective control and provide a way to engineer CSPs for RP-HPLC separation. This facilitates the synthesis of three robust chiral Zr(IV)-MOFs with a **flu** topology from the custom-designed 3,3′,5,5′-tetra(benzoate), -tetra(2-naphthoate), and -tetra(4-phenylbenzoate) ligands of enantiopure 2,2′-pentaethylene glycol-1,1′-biphenyl. Crown ether moieties are periodically aligned within the framework channels that are accessible for guest molecules. It should be noted that, due to the superior ability to complex with cationic species, chiral macrocyclic compounds including crown ethers can provide an enantioselective specific interaction with single enantiomer to resolve racemates.[11] By using acidic aqueous eluents, the Zr-MOF-packed HPLC columns afforded high resolution and enantioselectivity for the separation of a variety of racemates such as amino acids and amine drugs. The resolution abilities of Zr-MOFs can be tuned by modifying pore sizes through alteration of the linker lengths. The different interactions between crown ether groups of the Zr-MOF and racemates were revealed by DFT calculations and accounted for the chiral separation capacity.

RESULTS AND DISCUSSION

Synthesis and Characterization. The tetracarboxylate ligands H_4L^1–H_4L^3 were prepared from enantiopure 6,6′-dimethyl-3,3′-*tert*-butyl-5,5′-dibro-1,1′-biphenyl-2,2′-diol in several steps. The solvothermal reactions of $ZrOCl_2{\cdot}8H_2O$ and H_4L^1, H_4L^2, or H_4L^3 in DMF with formic acid or trifluoroacetic acid (TFA) as modulating agent at 120 °C for 24 h afforded colorless octahedral crystals of $[Zr_6O_4(OH)_8(H_2O)_4(L^1)_2]$ (**CE-1**), $[Zr_6O_4(OH)_8(H_2O)_4(L^2)_2]$ (**CE-2**), or $[Zr_6O_4(OH)_8(H_2O)_4(L^3)_2]$ (**CE-3**), respectively. The prod-

https://dx.doi.org/10.1021/jacs.0c11276
J. Am. Chem. Soc. XXXX, XXX, XXX–XXX

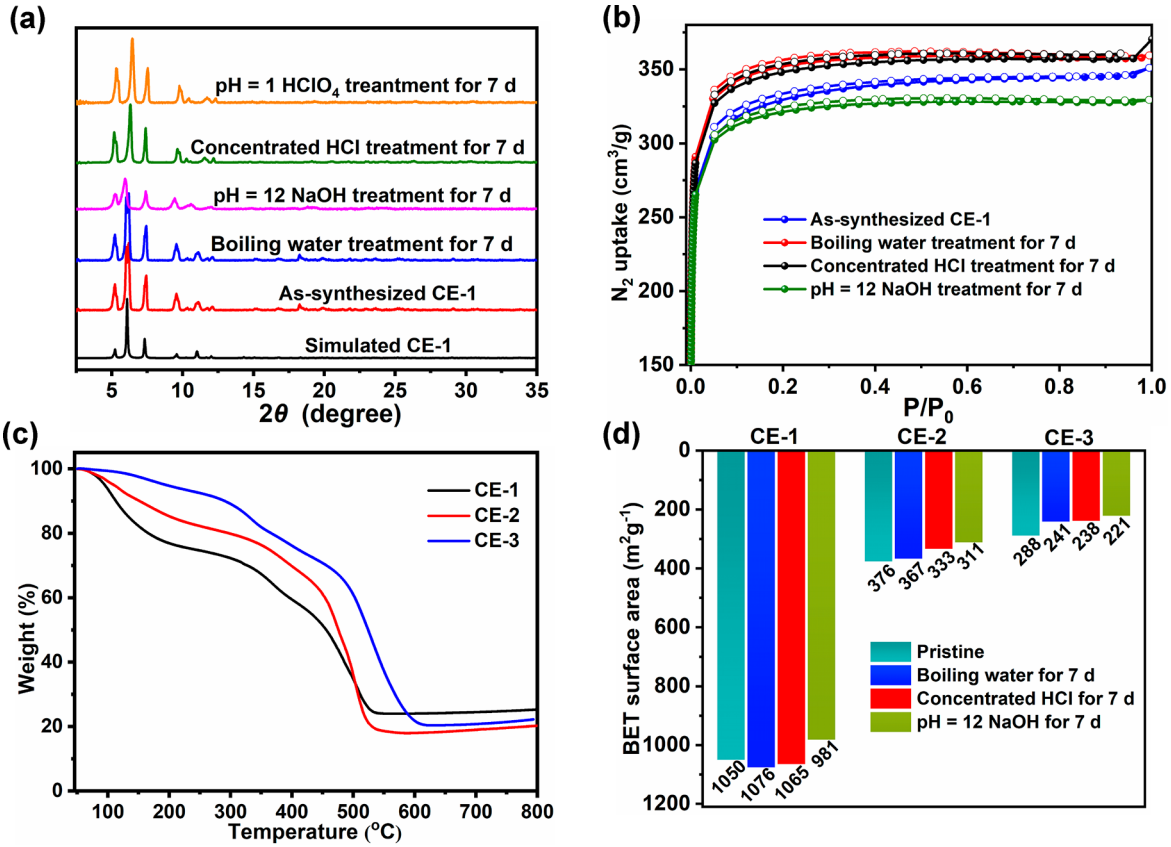

Figure 2. (a) PXRD patterns and (b) N_2 adsorption isotherms for **CE-1** under different conditions. (c) TGA curves for **1**−**3**. (d) BET surface areas for **1**−**3** under different conditions.

ucts are insoluble in water and common solvents. They have been thoroughly characterized by elemental analysis, FT-IR spectra, and thermogravimetric analysis (TGA). The phase purity of them was confirmed by comparison of their experimental and simulated powder X-ray diffraction (PXRD) patterns.

Single-crystal X-ray diffraction (SCXRD) revealed that **1**−**3** crystallize in the same space group and share identical topological structures. **CE-1** crystallizes in the chiral space group $P2_12_12_1$, with one of the formula in the asymmetric unit. Six Zr atoms are assembled into an octahedral $Zr_6(\mu_3\text{-}OH)_4(\mu_3\text{-}O)_4$ core by four μ_3-O and four μ_3-OH groups, with terminal positions occupied by four − OH and four water molecules. Each $\mathbf{L^1}$ connected four hexanuclear Zr clusters via four bidentate carboxylate groups to form a (4,8)-connected **flu** framework (Figure 1a).[10] Because of the high symmetry of the framework and disordered crown ether units, the precise positions of crown ether groups cannot be modeled by SCXRD. Thus, we used Material Studio to model the position of the crown ether groups inside the cavities. The ^{1}H NMR spectrum of the digested **CE-1** also clearly confirmed the existence of crown ether units inside the MOF (Figure S1). A dodecahedral cage with a cavity of dimensions about 12.5 × 24.9 × 26.9 Å^3 is constructed from six Zr_6 clusters occupying the vertices and eight $\mathbf{L^1}$ linkers riding on the faces (Figure 1b and d). The cage cavities are periodically decorated with the crown ether groups of biphenol backbones that are accessible to guest molecules. The dodecahedral cage is surrounded by 12 adjacent cages via sharing faces, thus generating a 3D porous structure (Figure 1c). **CE-2** and **CE-3** are isostructural to **CE-1** but with larger pore size due to the extension of the peripheral arms of the ligands. Similar to **CE-1**, the Zr_6 clusters were cross-linked by $\mathbf{L^2}$ and $\mathbf{L^3}$ units to form a **flu** network featuring a larger cavity with sizes of about 12.5 × 27.8 × 36.1 and 17.3 × 35.5 × 39.6 Å^3 for **CE-2** and **CE-3**, respectively (Figure 1e and f). The crown ether parts were also modeled by Material Studio, and the ^{1}H NMR spectrum of the digested samples clearly indicated the existence of the crown ether moieties (Figures S2 and S3). As a result of the different lengths of the tetracarboxylate ligands, the crown ether MOF series is highly porous with a tunable void space with 73.3%, 75.9%, and 84.3%, as calculated by PLATON for **1**−**3**, respectively.[12] As shown in Figure S5, **1**−**3** have tunable opening channels of 8.5 × 14.9, 9.9 × 19.5, and 13.7 × 24.2 Å^2 along the *a* axis and of 8.5 × 9.0, 8.9 × 9.9, and 11.4 × 13.7 Å^2 along the *c* axis, respectively.

Solid-state circular dichroism (CD) of **1**-**3** spectra built from (*R*)- or (*S*)-enantiomers of $H_4\mathbf{L}$ are mirror images of each other, revealing their enantiomeric nature (Figure S6). Scanning electron microscopy (SEM) images showed **1**−**3** possess a uniform octahedral morphology (Figure S10). The permanent porosity of **CE-1** was demonstrated by N_2 adsorption measurement at 77 K. After desolvation of the acetone-exchanged sample by heating at 120 °C under dynamic vacuum overnight, it still remained of high crystallinity and exhibited a type I sorption behavior, with a Brunauer−Emmett−Teller (BET) surface area of 1016 m^2 g^{-1} (Figure 2b). In contrast, **CE-2** and **CE-3** exhibited lower BET values of 375 and 287 m^2 g^{-1}, probably due to the distorted pore structure after solvent removal (Figure S9). This

https://dx.doi.org/10.1021/jacs.0c11276
J. Am. Chem. Soc. XXXX, XXX, XXX−XXX

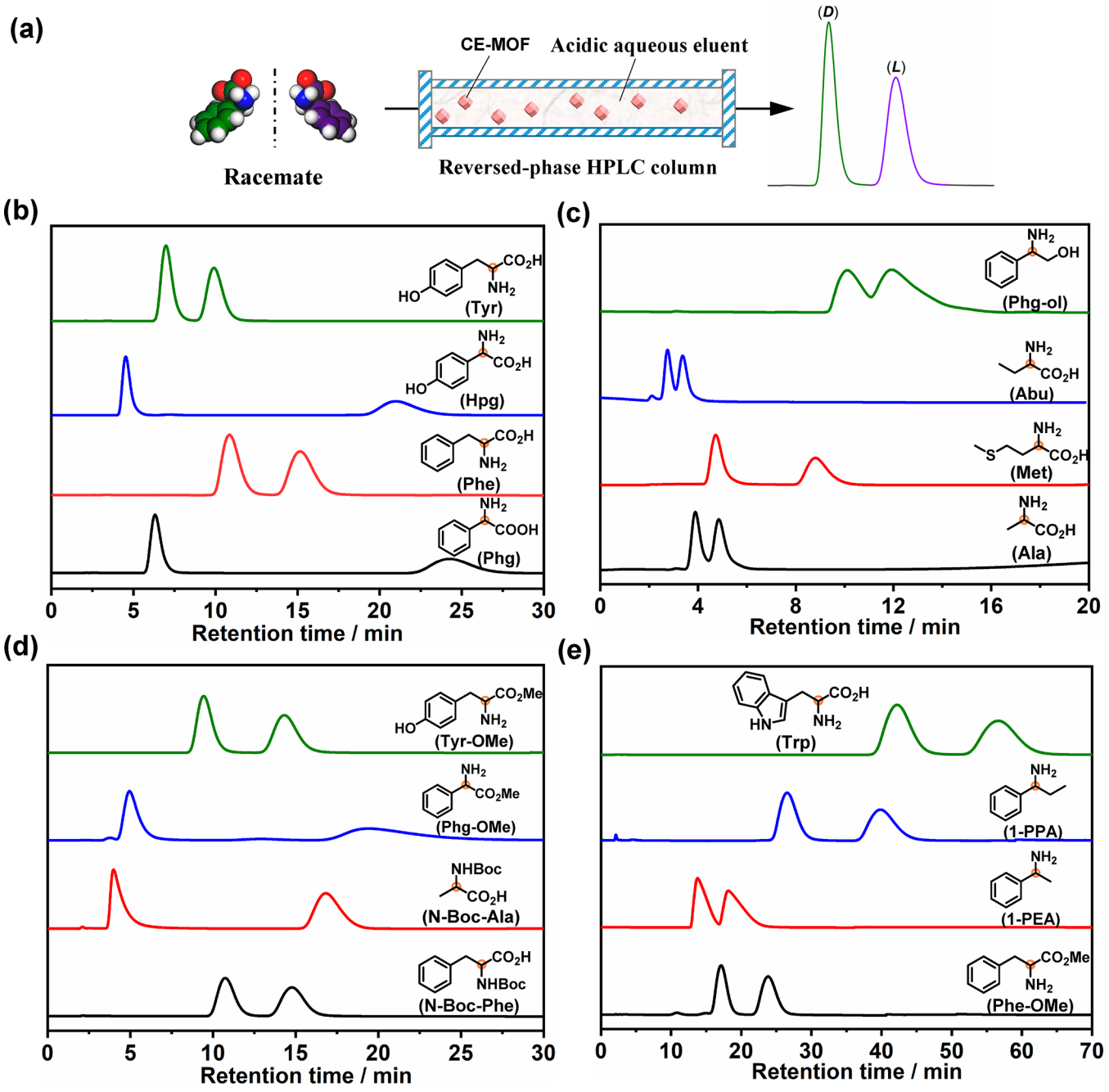

Figure 3. (a) Schematic illustration of RP-HPLC separation by CE-MOF packed column. (b–e) Chromatograms for the separation of 16 racemates with **CE-1** packed column (mobile phase pH = 1 $HClO_4$ (aq), 0.3 mL/min flow rate, detection wavelength 220 nm, temperature 25 °C).

phenomenon is often observed in highly porous MOFs.[13] Dye uptake experiments were then used to certify the structural integrity of the CMOFs in solution. **1**–**3** can adsorb 2.3, 3.8, and 4.6 methyl orange (MO, ~1.47 nm × 0.53 nm) per formula unit, and 1.7, 2.3, and 3.6 rhodamine 6G (R6G, ~1.43 nm × 1.61 nm) in MeOH, respectively (Table S1). The above results implied that the structural integrity and open channels of the three MOFs are maintained in solution.

Chemical Stability. As expected, **1**–**3** showed excellent thermal stability. TGA showed that guest molecules within them could be removed in the temperature ranging from 80 to 200 °C, and the frameworks started to decompose at about 400 °C (Figure 2c).

The chemical stability of the frameworks was studied by PXRD and N_2 adsorption after treatment in boiling water, concentrated HCl (aq), and pH = 12 NaOH (aq) at rt for 1 week, as well as dye uptake measurements. As shown in Figures 2a and S8, PXRD patterns of **1**–**3** after these treatments remained intact, suggesting that no phase transition or framework collapse happened. The minor shift of peaks for **CE-2** and **CE-3** can be explained by a certain degree of the framework flexibility. Both of the as-treated CMOFs retained their permanent porosity, as evidenced by BET measurements (Figure 2d). Dye uptake measurements showed the samples of **1**–**3** after these treatments could adsorb 1.6/1.4/1.3, 2.4/2/1.8, and 3.4/3/2.8 R6G per formula unit, respectively,

https://dx.doi.org/10.1021/jacs.0c11276
J. Am. Chem. Soc. XXXX, XXX, XXX−XXX

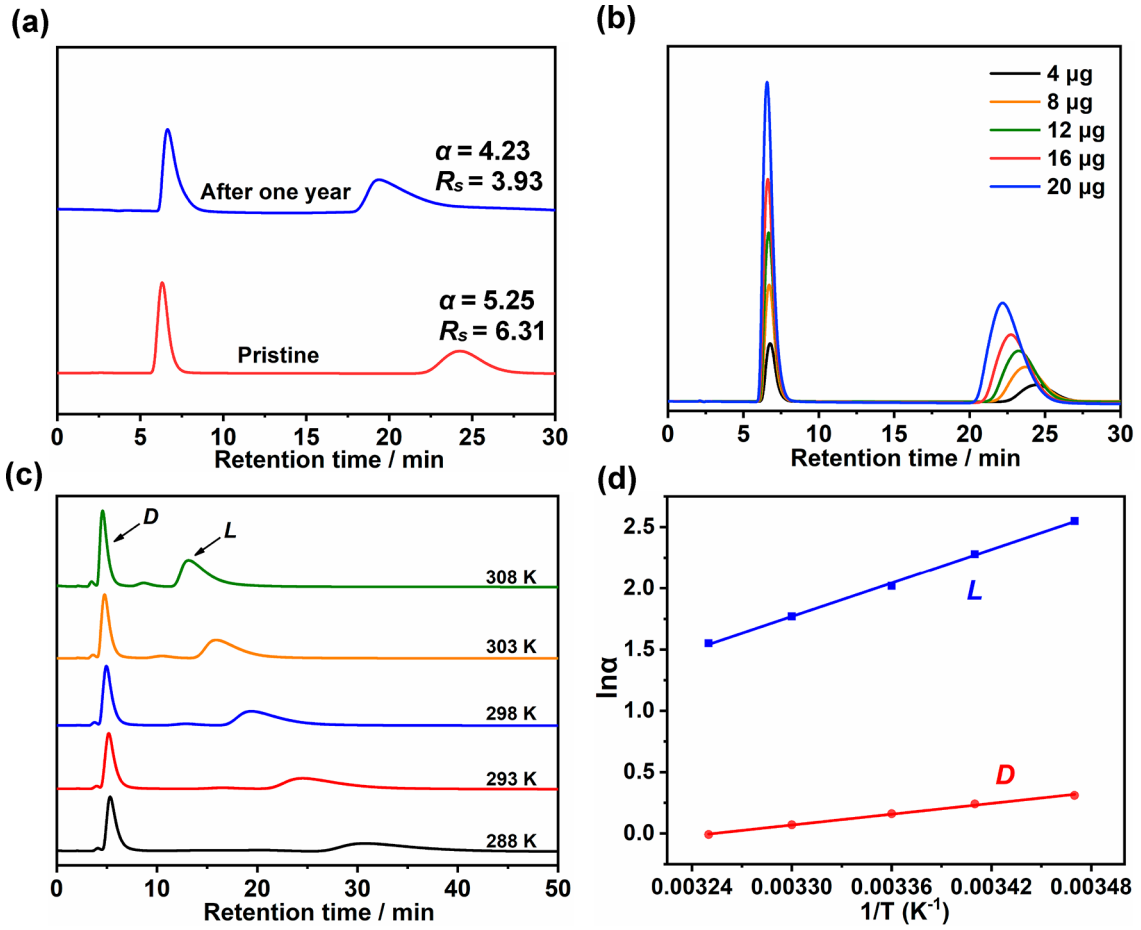

Figure 4. (a) HPLC chromatograms of racemic Phg on the **CE-1** packed column after being used for 4000 injections after 1 year. (b) Effect of injected mass of Phg on the **CE-1** packed column. The injected mass was increased from 4 to 20 μg. (c) HPLC chromatograms of Phg-OMe on the **CE-1** packed column at 288−308 K. (d) The van't Hoff plots for D- and L-Phg-OMe.

comparable to the untreated sample, indicative of the structural integrity (Table S2).

The high chemical stability of these three Zr-MOFs can be ascribed to the following reasons: First, the highly charged Zr(IV) ions can polarize the Zr−O coordination bond that results in a strong bonding between Zr(IV) and carboxylate oxygens in the ligands.[9a] Second, the methyl and crown ether groups at the *ortho* positions of the central two aryl rings prevent the free rotation of the C−C linkages to rigidify the linker and thus further improve the framework stability.[14a] Third, the electron-donating nature of the methyl and crown ether groups leads to an increase of electron density of carboxylate oxygens, which can enhance the Zr−O bond strength.[10a,14b] The excellent stability of the Zr-CMOFs makes them attractive CSPs for enantioselective chromatographic separation.

RP-HPLC Enantioseparation. Inspired by the excellent stability, large porosity, and abundant chiral crown ether groups of the Zr-based MOFs, we utilized them as CSPs for RP-HPLC separations. However, the columns packed with the pure MOF powders exhibit very high back-pressure (>20 MPa), and so we prepared the CSPs of Zr-MOFs mixed with reverse phase C_{18} silica gel. The **CE-1** packed column was prepared by loading the mixture of **CE-1** and C_{18} silica gel in methanol/water (1:9, v/v) into a 25 cm long × 2.1 mm internal diameter (i.d.) stainless steel column under a pressure of 5000 psi. Prior to data collection, the column was conditioned with HPLC-grade water at a flow rate of 0.2 mL/min for 6 h. The performance of the CSP was first investigated by resolving phenylglycine (Phg) (Figure 3a), which is an essential intermediate and shows great potential value in the areas such as pharmacies, food additives, and fine chemicals.[15] After the separation conditions including the mobile phase compositions (acid and pH) and flow rate were optimized, racemic Phg was successfully baseline separated on the **CE-1**-based CSP with pH = 1 $HClO_4$ (aq) as the mobile phase at a flow rate of 0.3 mL/min at 25 °C (Figure S12). An excellent selectivity factor (α = 5.25) and chromatographic resolution factor (R_s = 6.31) were achieved, and the elution sequence was the D-enantiomer followed by the L-enantiomer (Figure 3b). In this HPLC system, the back-pressure is about 9 MPa. It is also worth noting that the mobile phase and flow rate can significantly affect the retention time, resolution, and selectivity (Figure S12).

To expand the scope of the analytes, we examined seven other amino acids including phenylalanine (Phe), 4-hydroxyphenylglycine (Hpg), tyrosine (Tyr), tryptophan (Trp), alanine (Ala), methionine (Met), and 2-aminobutyric acid (Abu). Encouragingly, all of them were completely resolved on the **CE-1**-based CSPs with α/R_s = 1.49/1.85, 7.77/6.59, 1.60/1.99, 1.36/1.85, 1.53/1.23, 2.36/3.51, and 1.66/1.02, respectively (Figure 3b, c, and e). Furthermore, amino acid derivatives, such as N-protected amino acids (N-Boc-Ala and N-Boc-Phe), amino esters (Phg-OMe, Tyr-OMe, and Phe-

https://dx.doi.org/10.1021/jacs.0c11276
J. Am. Chem. Soc. XXXX, XXX, XXX−XXX

Table 1. Comparison of the Separation Performance of Six Racemic Amino Acids by RP-HPLC Columns Packed with CE-1, Me_4L^1, OET-1 (Analogue of CE-1 with −OEt Groups), and Several Commercial CSPs[a]

	CE-1[b]		Me_4L^1[b]		OET-1[b]		CROWN-PAK CR(+)[17a,c]		Chirosil RCA(+)[17b,d]		Chirobiotic T[17c,e]	
analytes	α	R_s	α	R_s	α	R_s	α	R_s	α	R_s	α	R_s
Phg	5.25	6.31	2.01	1.82	1.00	[f]	3.97	14.27	2.25	6.46	3.10	2.90
Phe	1.49	1.85	1.25	1.56	1.00	[f]	1.20	2.69	1.48	2.31	1.50	2.00
Tyr	1.60	1.99	1.28	1.72	1.00	[f]	1.16	2.22	1.44	2.00	1.50	1.90
Trp	1.36	1.85	1.19	0.91	1.00	[f]	[g]	[g]	1.44	2.15	1.50	2.20
Ala	1.45	1.99	1.25	1.22	1.00	[f]	1.65	1.66	1.28	1.33	1.80	2.90
Met	2.36	3.51	1.83	3.37	1.00	[f]	1.85	6.75	1.39	2.06	2.20	3.30

[a]Separation factor $\alpha = (t_{R2} - t_M)/(t_{R1} - t_M)$, resolution factor $R_s = 2(t_{R2} - t_{R1})/(w_1 + w_2)$. t_M, the column void time, is determined by using 1,3,5-tri-*tert*-butylbenzene as analyte. t_{R1} and t_{R2} are the retention times, and w_1 and w_2 are the peak widths of the peaks. [b]Mobile phase pH = 1 $HClO_4$ (aq), 0.3 mL/min flow rate, detection wavelength 220 nm, temperature 25 °C. [c]Mobile phase pH = 2 $HClO_4$ (aq), 0.5 mL/min flow rate, detection wavelength set to 200 or 254 nm, temperature 18 °C. [d]Mobile phase 80% CH_3OH in H_2O + H_2SO_4 (10 mM), 0.5 mL/min flow rate, detection wavelength set to 210 nm, temperature 20 °C. [e]Mobile phase CH_3OH−H_2O (60−40, v/v), 1.0 mL/min flow rate, detection wavelength set to 210 nm. [f]Could not be separated. [g]Not reported.

OMe), and amino alcohols (Phg-ol), can also be separated, affording α/R_s = 1.23/0.63 to 3.23/10.21 (Figure 3c−e). Furthermore, some unprotected amines such as 1-phenylethylamine (1-PEA) and 1-phenylpropylamine (1-PPA) can be baseline separated with α/R_s = 1.38/0.96 and 1.54/2.34, respectively (Figure 3e). Importantly, except for Trp and 1-PPA, all other substrates were separated on the **CE-1** column within 30 min. The short separation time enables a fast analysis of the samples, which is highly efficient and time-saving for enantioselective separation.

Also, we prepared columns packed with **CE-2** and **CE-3** using the same procedure as for **CE-1** to compare their separation behaviors toward amino acids. Both columns can separate the racemic amino acids with α/R_s = 1.08/0.33 to 4.16/4.04, which are lower than the values for the **CE-1** column (Figure S14a and Table S5). In particular, both the resolution and the separation factor decreased as the channel sizes of the frameworks increased. The different separation performance of **1**−**3** may be ascribed to the different levels of asymmetric induction ability caused by the various channel sizes and aryl substituents.

The durability of the **CE-1** column was evaluated by studying its performance after 1 year of shelf life and over 4000 multiple injections (Figure 4a). There was a slight decrease of separation performance with α/R_s reduced from 5.25/6.31 to 4.23/3.93. PXRD studies indicated that the recovered samples of **CE-1** after HPLC measurement remained crystalline and structurally intact (Figure S8). Furthermore, the repeatability of **CE-1** column was examined by five replicate separations of Phg and Phe-OMe (Figure S14f and g). The RSD (relative standard deviation) values of selectivity factor, peak area, peak height, and theoretical plate number were calculated to be less than 2.0%, further confirming the separation stability of the column (Tables S6 and S7). Also, we prepared another **CE-1** packed column by using the same procedure. The two separated **CE-1** packed columns exhibited similar separation performance (Figure S14h and Table S8) and demonstrated the good preparation reproducibility of this method. It is worth mentioning that a variety of chiral porous materials including CMOFs and chiral covalent organic frameworks (CCOFs) have been explored as CSPs for chiral HPLC separation, but they typically suffer low stability and narrow analyte scope.[8,16] Moreover, they all used organic solvents as eluents that bring serious pollution. To the best of our knowledge, this represents the first report utilizing MOFs as CSPs for RP-HPLC. As shown in Table 1, the resolution abilities of **CE-1**-CSP are comparable to or even better than those of the three widely used commercial chiral columns CROWNPAK CR(+), Chirosil RCA(+), and Chirobiotic T, which are derived from (*S*)-(3,3′-diphenyl-1,1′-binaphthyl)-20-crown-6, (+)-(18-crown-6)-2,3,11,12-tetracarboxylic acid, and teicoplanin, respectively.[17]

A demonstration of the utility of this MOF-based CSP is presented in the separation of drug enantiomers that is highly desired in pharmaceutical, agricultural, and fine chemical industries. Baclofen, a chemical analogue of γ-aminobutyric acid, is widely used for the treatment of spinal cord injury-induced spasm.[18] The *R*-enantiomer is the actual active species, although the racemic compound is used in clinic practice.[18b] We used the **CE-1** packed column to separate racemic baclofen. To our delight, racemic baclofen can be baseline separated with α/R_s = 1.85/3.66 (Figure 5a). Another

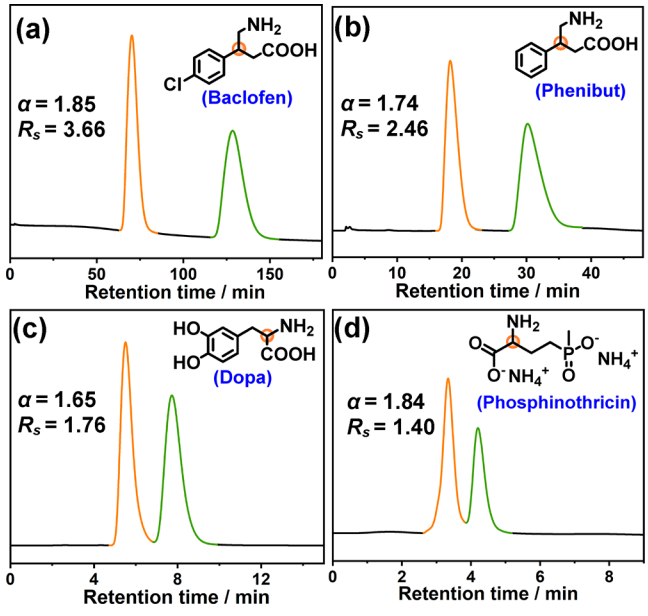

Figure 5. HPLC chromatograms of the four racemic drugs including baclofen, phenibut, Dopa, and phosphinothricin by the **CE-1** packed column (mobile phase pH = 1 $HClO_4$ (aq), 0.3 mL/min flow rate, detection wavelength 220 nm, temperature 25 °C).

https://dx.doi.org/10.1021/jacs.0c11276
J. Am. Chem. Soc. XXXX, XXX, XXX−XXX

γ-aminobutyric acid, phenibut, can also be well separated affording α/R_s = 1.74/2.46 (Figure 5b). 3,4-Dihydroxyphenylalanine (Dopa), a drug for the treatment of Pakinson's disease, can be separated with α/R_s = 1.65/1.76 (Figure 5c). Besides, **CE-1**-based CSP can also separate the agricultural chemical glufosinate ammonium (phosphinothricin) affording α/R_s = 1.84/1.40 (Figure 5d). These results demonstrate the potential versatility of **CE-1** for the separation of diverse chiral drugs.

To gain further insight into the separation of chiral molecules, we prepared a column packed with Me_4L^1 and evaluated its chiral recognition ability as CSP. The as-prepared column can separate amino acids with good to excellent separation resolution, affording α/R_s = 1.19/0.91 to 1.83/3.37 (Figure S14b and Table 1). This suggested that the crown ether moieties play a significant role in the separation process. However, as compared to the **CE-1** column, the Me_4L^1 column typically showed lower separation factor and resolution. This may be attributed to the fact that the framework can exert extra confinement environment and thus lead to an enhancement of enantiospecific interaction. To examine the importance of crown ether moieties, we have synthesized an isoreticular framework **OET-1** with OEt groups instead of crown ether moieties. **OET-1** also showed excellent chemical stability toward different harsh conditions (Figures S8 and S9). However, the **OET-1** packed column cannot separate any of the analytes under the same conditions (Figure S14c and Table 1). Besides, control experiments showed that the pure C_{18} column does not have the separation ability toward amino acids (Figure S14e). This proves the significant role of crown ether groups in enantioselective recognition. To study the confined space effect of the framework, we used the bulky 3,5-dibenzyloxy-1-phenylalanine methyl ester with a size of 14 Å × 16 Å as the analyte (Figure S11). It can be separated in the Me_4L^1 packed column with α/R_s = 1.21/1.19, but cannot be baseline separated in the column packed by **CE-1** with a maximum channel size of 8.5 Å × 14.9 Å (Figure S14d). Taken together, we can speculate that the crown ether groups combined with the confined space of the crystalline framework exert an important influence in chiral recognition.

To examine the loading capacity of the CSP without compromising resolution, a loading test was carried out using different inject masses. When the loading was increased from 4 to 20 μg of each racemate, Phg can still achieve baseline separation (Figure 5b). Besides, the chromatographic peak area of each single antipode rises in line with the increase of the injected mass (Figure S13). It is observed that the retention time of the enantiomer became closer with increasing injection mass, although it did achieve baseline resolution. The result may be due to the strong interaction between amine species and crown ether groups.

To better understand the separation process, the thermodynamics of Phg-OMe separation was investigated at temperatures ranging from 288 to 308 K (Figure 5c). It was observed that the retention times of the analytes were decreased as the column temperature increased. The van't Hoff plots for the analytes exhibited excellent linear correlation, and this suggested no changes of the interactions during the separation process (Figure 5d). The molar adsorption enthalpy/entropy changes $\Delta_{ads}H_m/\Delta_{ads}H_m$ of (D)- and (L)-protonated Phg-OMe are −3.64 and −11.30 kJ/mol, respectively. The differences $\Delta(\Delta_{ads}H_m)_{L-D}$ and $\Delta(\Delta_{ads}S_m)_{L-D}$ are calculated as −7.66 kJ/mol and −70.66 J/(mol K), and this suggests that the separation process is enthalpy driven. In addition, the adsorption enthalpy results are consistent with the order of retention times and the elution sequence of the D- and L-enantiomers.

To microscopically elucidate the interactions between the crown ether group in (*S*)-**CE-1** and L/D-protonated Phg-OMe, density functional theory (DFT) calculations were performed. As shown in Figure S15, there are two configurations of the crown ether groups in (*S*)-**CE-1** with the dihedral angles of two center phenyl rings at about 64° or 112°, respectively. However, geometric optimization of the host models (Figures S17 and S18) suggests that only the configuration with the dihedral angles of two center phenyl rings at 64° could provide adequate space for the favorable binding of L/D-enantiomers. Figure 6 depicts the simplified structures of the most stable

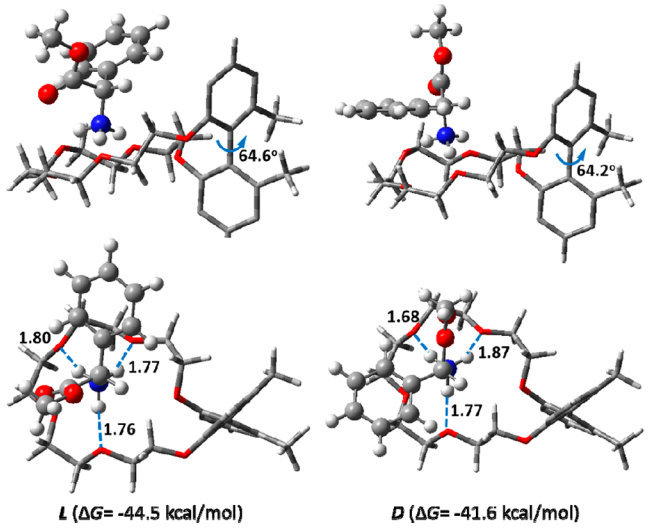

Figure 6. Side (upper) and top (lower) views of the lowest-energy structures of L- and D-protonated Phg-OMe with (*S*)-**CE-1**. The Gibbs binding energies at 298 K are indicated in the parentheses. The lengths (in Å) of hydrogen bonds involved in the host−guest interactions and the dihedral angles of the two center phenyl rings are labeled. The MOF frameworks surrounding the host−guest complexes are omitted for clarity. C, gray; H, white; O, red; and N, dark blue.

conformers of L/D-protonated Phe-OMe with (*S*)-**CE-1**. The corresponding structures with the surrounding frameworks can be found in Figure S20. Both the L- and the D-protonated Phg-OMe bind to the crown ether group in (*S*)-**CE-1** through three hydrogen bonds. At room temperature, the predicted Gibbs binding energy for the L-enantiomer is 2.9 kcal/mol higher than that for the D-enantiomer. This demonstrates a marked chiral recognition of the L-enantiomer relative to the D-enantiomer by (*S*)-**CE-1**, as attributed to the favorable host−guest binding through hydrogen bonds at optimum distances and collinear orientations in the confined framework.

CONCLUSIONS

We have designed and prepared three chiral crown ether embedded Zr-MOFs with a **flu** network topology based on three enantiopure 1,1′-biphenol-derived tetracarboxylate linkers. The obtained porous Zr-MOFs displayed highly chemical stability and can serve as robust CSPs for RP-HPLC separation. Thus, a range of racemic N-containing compounds including amino acids, amino esters, and some drugs were well separated under acidic eluent conditions, with separation

https://dx.doi.org/10.1021/jacs.0c11276
J. Am. Chem. Soc. XXXX, XXX, XXX−XXX

performances comparable to or even superior to those of some commercial CSPs. Controlled experiments and DFT calculations revealed that chiral crown ether moieties combined with the confined space account for the efficient separation. This work thus advances MOFs as a platform for chiral resolution in reversed-phase liquid chromatography and will promote the design of more robust Zr-MOFs for the recognition and separation of racemic fine chemicals and pharmaceuticals.

■ ASSOCIATED CONTENT

Supporting Information

The Supporting Information is available free of charge at https://pubs.acs.org/doi/10.1021/jacs.0c11276.

Experimental procedures and characterization data (PDF)

X-ray crystallographic data for **CE-1** (CIF)

X-ray crystallographic data for **CE-2** (CIF)

X-ray crystallographic data for **CE-3** (CIF)

■ AUTHOR INFORMATION

Corresponding Authors

Yan Liu − *School of Chemistry and Chemical Engineering, Frontiers Science Center for Transformative Molecules and State Key Laboratory of Metal Matrix Composites, Shanghai Jiao Tong University, Shanghai 200240, China;* orcid.org/0000-0002-7560-519X; Email: liuy@sjtu.edu.cn

Jianwen Jiang − *Department of Chemical and Biomolecular Engineering, National University of Singapore, Singapore 117576, Singapore;* orcid.org/0000-0003-1310-9024; Email: chejj@nus.edu.sg

Yong Cui − *School of Chemistry and Chemical Engineering, Frontiers Science Center for Transformative Molecules and State Key Laboratory of Metal Matrix Composites, Shanghai Jiao Tong University, Shanghai 200240, China;* orcid.org/0000-0003-1977-0470; Email: yongcui@sjtu.edu.cn

Authors

Hong Jiang − *School of Chemistry and Chemical Engineering, Frontiers Science Center for Transformative Molecules and State Key Laboratory of Metal Matrix Composites, Shanghai Jiao Tong University, Shanghai 200240, China;* orcid.org/0000-0002-4118-5297

Kuiwei Yang − *Department of Chemical and Biomolecular Engineering, National University of Singapore, Singapore 117576, Singapore*

Xiangxiang Zhao − *School of Chemistry and Chemical Engineering, Frontiers Science Center for Transformative Molecules and State Key Laboratory of Metal Matrix Composites, Shanghai Jiao Tong University, Shanghai 200240, China*

Wenqiang Zhang − *School of Chemistry and Chemical Engineering, Frontiers Science Center for Transformative Molecules and State Key Laboratory of Metal Matrix Composites, Shanghai Jiao Tong University, Shanghai 200240, China*

Complete contact information is available at: https://pubs.acs.org/10.1021/jacs.0c11276

Notes

The authors declare no competing financial interest.

■ ACKNOWLEDGMENTS

This work was financially supported by the National Science Foundation of China (grant nos. 21620102001, 91856204, 91956124, and 21875136), the National Key Basic Research Program of China (2016YFA0203400), the Key Project of Basic Research of Shanghai (17JC1403100 and 18JC1413200), the Shanghai Rising-Star Program (19QA1404300), and the China Postdoctoral Science Foundation (2020M681280). We thank the staff from the BL17B beamline of the National Facility for Protein Science in Shanghai (NFPS) at the Shanghai Synchrotron Radiation Facility, for assistance during data collection.

■ REFERENCES

(1) (a) Kasprzyk-Hordern, B. Pharmacologically Active Compounds in the Environment and Their Chirality. *Chem. Soc. Rev.* **2010**, *39*, 4466. (b) Liu, Y.; Xuan, W.; Cui, Y. Engineering Homochiral Metal-Organic Frameworks for Heterogeneous Asymmetric Catalysis and Enantioselective separation. *Adv. Mater.* **2010**, *22*, 4112.

(2) (a) Ward, T. J.; Ward, K. D. Chiral Separations: a Review of Current Topics and Trends. *Anal. Chem.* **2012**, *84*, 626. (b) Okamoto, Y.; Ikai, T. Chiral HPLC for Efficient Resolution of Enantiomers. *Chem. Soc. Rev.* **2008**, *37*, 2593.

(3) (a) Zuvela, P.; Skoczylas, M.; Liu, J. J.; Baczek, T.; Kaliszan, R.; Wong, M. W.; Buszewski, B. Column Characterization and Selection Systems in Reversed-Phase High-Performance Liquid Chromatography. *Chem. Rev.* **2019**, *119*, 3674. (b) Ikai, T.; Okamoto, Y. Structure Control of Polysaccharide Derivatives for Efficient Separation of Enantiomers by Chromatography. *Chem. Rev.* **2009**, *109*, 6077. (c) Sancho, R.; Minguillón, C. The Chromatography Separation of Enantiomers through Nanoscale Design. *Chem. Soc. Rev.* **2009**, *38*, 797.

(4) (a) Okamoto, Y.; Yashima, E. Polysaccharide Derivatives for Chromatographic Separation of Enantiomers. *Angew. Chem., Int. Ed.* **1998**, *37*, 1020. (b) Bicchi, C.; D'Amato, A.; Rubiolo, P. Cyclodextrin Derivatives as Chiral Selectors for Direct Gas Chromatographic Separation of Enantiomers in the Essential Oil, Aroma and Flavor Fields. *J. Chromatogr. A* **1999**, *843*, 99. (c) Shen, J.; Okamoto, Y. Efficient Separation of Enantiomers Using Stereoregular Chiral Polymers. *Chem. Rev.* **2016**, *116*, 1094.

(5) (a) Furukawa, H.; Cordova, K. E.; O'Keeffe, M.; Yaghi, O. M. The Chemistry and Applications of Metal-Organic Frameworks. *Science* **2013**, *341*, 974. (b) Hendon, C. H.; Reith, A. J.; Korzyński, M. D.; Dincă, M. Grand Challenges and Future Opportunities for Metal-Organic Frameworks. *ACS Cent. Sci.* **2017**, *3*, 554. (c) Kirchon, A.; Feng, L.; Drake, H. F.; Joseph, E. A.; Zhou, H. C. From Fundamentals to Applications: A Toolbox for Robust and Multifunctional MOF Materials. *Chem. Soc. Rev.* **2018**, *47*, 8611. (d) Chen, Z.; Li, P.; Anderson, R.; Wang, X.; Zhang, X.; Robison, L.; Redfern, L. R.; Moribe, S.; Islamoglu, T.; Gómez-Gualdrón, D. A.; Yildirim, T.; Stoddart, J. F.; Farha, O. K. *Science* **2020**, *368*, 297. (e) Cao, C.-C.; Chen, C.-X.; Wei, Z.-W.; Qiu, Q.-F.; Zhu, N.-X.; Xiong, Y.-Y.; Jiang, J.-J.; Wang, D.; Su, C.-Y. Catalysis through Dynamic Spacer Installation of Multivariate Functionalities in Metal-Organic Frameworks. *J. Am. Chem. Soc.* **2019**, *141*, 2589. (f) Xu, H.; Hu, J.; Wang, D.; Li, Z.; Zhang, Q.; Luo, Y.; Yu, S.-H.; Jiang, H.-L. Visible-Light Photoreduction of CO_2 in a Metal-Organic Framework: Boosting Electron-Hole Separation via Electron Trap States. *J. Am. Chem. Soc.* **2015**, *137*, 13440.

(6) For MOFs as stationary phases for chromatographic separation, see reviews: (a) Gu, Z.-Y.; Yang, C.-X.; Chang, N.; Yan, X.-P. Metal-Organic Frameworks for Analytical Chemistry: From Sample Collection to Chromatographic Separation. *Acc. Chem. Res.* **2012**, *45*, 734. (b) Duerinck, T.; Denayer, J. F. M. Metal-Organic

Frameworks as Stationary Phases for Chiral Chromatographic and Membrane Separations. *Chem. Eng. Sci.* **2015**, *124*, 179. (c) Li, X.; Chang, C.; Wang, X.; Bai, Y.; Liu, H. Applications of Homochiral Metal-Organic Frameworks in Enantioselective Adsorption and Chromatography Separation. *Electrophoresis* **2014**, *35*, 2733. (d) Zhang, J.; Chen, J.; Peng, S.; Peng, S.; Zhang, Z.; Tong, Y.; Miller, P. W.; Yan, X.-P. Emerging Porous Materials in Confined Spaces: From Chromatographic Applications to Flow Chemistry. *Chem. Soc. Rev.* **2019**, *48*, 2566.

(7) For chiral MOFs for GC separation, see: (a) Xie, S.-M.; Zhang, Z.-J.; Wang, Z.-Y.; Yuan, L.-M. Chiral Metal−Organic Frameworks for High-Resolution Gas Chromatographic Separations. *J. Am. Chem. Soc.* **2011**, *133*, 11892. (b) Zhang, S.-Y.; Yang, C.-X.; Shi, W.; Yan, X.-P.; Cheng, P.; Wojtas, L.; Zaworotko, M. J. A Chiral Metal-Organic Material that Enables Enantiomeric Identification and Purification. *Chem.* **2017**, *3*, 281. (c) Kou, W.-T.; Yang, C.-X.; Yan, X.-P. Post-Synthetic Modification of Metal-Organic Frameworks for Chiral Gas Chromatography. *J. Mater. Chem. A* **2018**, *6*, 17861.

(8) For chiral MOFs for HPLC separation, see: (a) Padmanaban, M.; Müller, P.; Lieder, C.; Gedrich, K.; Grünker, R.; Bon, V.; Senkovska, I.; Baumgärtner, S.; Opelt, S.; Paasch, S.; Brunner, E.; Glorius, F.; Klemm, E.; Kaskel, S. Application of a Chiral Metal-Organic Framework in Enantioselective Separation. *Chem. Commun.* **2011**, *47*, 12089. (b) Tanaka, K.; Muraoka, T.; Hirayama, D.; Ohnish, A. High Efficient Chromatographic Resolution of Sulfoxides Using a New Homochiral MOF-Silica Composite. *Chem. Commun.* **2012**, *48*, 8577. (c) Zhang, M.; Pu, Z.-J.; Chen, X.-L.; Gong, X.-L.; Zhu, A.-X.; Yuan, L.-M. Chiral Recognition of a 3D Chiral Nanoporous Metal-Organic Framework. *Chem. Commun.* **2013**, *49*, 5201. (d) Peng, Y.; Gong, T.; Zhang, K.; Lin, X.; Liu, Y.; Jiang, J.; Cui, Y. Engineering Chiral Porous Metal-Organic Frameworks for Enantioselective Adsorption and Separation. *Nat. Commun.* **2014**, *5*, 4406. (e) Kuang, X.; Ma, Y.; Su, H.; Zhang, J.; Dong, Y.-B.; Tang, B. High-Performance Liquid Chromatographic Enantioseparation of Racemic Drugs Based on Homochiral Metal-Organic Framework. *Anal. Chem.* **2014**, *86*, 1277. (f) Hartlieb, K. J.; Holcroft, J. M.; Moghadam, P. Z.; Vermeulen, N. A.; Algaradah, M. M.; Nassar, M. S.; Botros, Y. Y.; Snurr, R. Q.; Stoddart, J. F. CD-MOF A Versatile Separation Medium. *J. Am. Chem. Soc.* **2016**, *138*, 2292. (g) Corella-Ochoa, M. N.; Tapia, J. B.; Rubin, H. N.; Lillo, V.; González-Cobos, J.; Núñez-Rico, J. L.; Blastra, S. R. G.; Almora-Barrios, N.; Liedós, M.; Güell-Bara, A.; Cabezas-Giménez, J.; Escudero-Adán, E. C.; Vidal-Ferran, A.; Calero, S.; Reynolds, M.; Martí-Gastaldo, C.; Galán-Mascarós, J. R. Homochiral Metal-Organic Frameworks for Enantioselective Separations in Liquid Chromatography. *J. Am. Chem. Soc.* **2019**, *141*, 14306.

(9) (a) Cavka, J. H.; Jakobsen, S.; Olsbye, U.; Guillou, N.; Lamberti, C.; Bordiga, S.; Lillerud, K. P. A New Zirconium Inorganic Building Brick Forming Metal Organic Frameworks with Exceptional Stability. *J. Am. Chem. Soc.* **2008**, *130*, 13850. (b) Bai, Y.; Dou, Y.; Xie, L.; Rutledge, W.; Li, J.; Zhou, H. Zr-Based Metal-Organic Frameworks: Design, Synthesis, Structure, and Applications. *Chem. Soc. Rev.* **2016**, *45*, 2327.

(10) For Zr-MOFs with **flu** topology, see: (a) Jiang, H.; Zhang, W.; Kang, X.; Cao, Z.; Chen, X.; Liu, Y.; Cui, Y. Topology-Based Functionalization of Robust Chiral Zr-Based Metal-Organic Frameworks for Catalytic Enantioselective Hydrogenation. *J. Am. Chem. Soc.* **2020**, *142*, 9642. (b) Zhang, M.; Chen, Y. P.; Bosch, M.; Gentle, T., III; Wang, K.; Feng, D.; Wang, Z. U.; Zhou, H.-C. Symmetry-Guided Synthesis of Highly Porous Metal-Organic Frameworks with Fluorite Topology. *Angew. Chem., Int. Ed.* **2014**, *53*, 815. (c) Pang, J.; Yuan, S.; Qin, J.; Liu, C.; Lollar, C.; Wu, M.; Yuan, D.; Zhou, H.; Hong, M. Control the Structure of Zr-Tetracarboxylate Frameworks through Steric Tuning. *J. Am. Chem. Soc.* **2017**, *139*, 16939. (d) Yan, Y.; O'Connor, A. E.; Kanthasamy, G.; Atkinson, G.; Allan, D. R.; Blake, A. J.; Schröder, M. Unusual and Tunable Negative Linear Compressibility in the Metal-Organic Framework MFM-133(M) (M = Zr, Hf). *J. Am. Chem. Soc.* **2018**, *140*, 3952. (e) Angeli, G. K.; Batzavali, D.; Mavronasou, K.; Tsangarakis, C.; Stuerzer, T.; Ott, H.; Trikalitis, P. N. Remarkable Structural Diversity between Zr/Hf and Rare-Earth MOFs via Ligand Functionalization and the Discovery of Unique (4, 8)-c and (4, 12)-connected Frameworks. *J. Am. Chem. Soc.* **2020**, *142*, 15986.

(11) (a) Kyba, E. B.; Koga, K.; Sousa, L. R.; Siegel, M. G.; Cram, D. J. Chiral Recognition in Molecular Complexing. *J. Am. Chem. Soc.* **1973**, *95*, 2692. (b) Cram, D. J.; Cram, J. M. Design of Complexes Between Synthetic Hosts and Organic Guests. *Acc. Chem. Res.* **1978**, *11*, 8.

(12) Spek, A. L. Single-Crystal Structure Validation with the Program PLATON. *J. Appl. Crystallogr.* **2003**, *36*, 7.

(13) (a) Gong, W.; Chen, X.; Jiang, H.; Chu, D.; Cui, Y.; Liu, Y. Highly Stable Zr(IV)-Based Metal-Organic Frameworks with Chiral Phosphoric Acids for Catalytic Asymmetric Tandem Reactions. *J. Am. Chem. Soc.* **2019**, *141*, 7498. (b) Ma, L.; Falkowski, J. M.; Abney, C.; Lin, W. A Series of Isoreticular Chiral Metal-Organic Frameworks as a Tunable Platform for Asymmetric Catalysis. *Nat. Chem.* **2010**, *2*, 838.

(14) (a) Lv, X.-L.; Yuan, S.; Xie, L.-H.; Darke, H.-F.; Chen, Y.; He, T.; Dong, C.; Wang, B.; Zhang, Y.-Z.; Li, J.-R.; Zhou, H.-C. Ligand Rigidification for Enhancing the Stability of Metal-Organic Frameworks. *J. Am. Chem. Soc.* **2019**, *141*, 10283. (b) Wang, B.; Lv, X.-L.; Feng, D.; Xie, L.-H.; Zhang, J.; Li, M.; Xie, Y.; Li, J.-R.; Zhou, H.-C. Highly Stable Zr(IV)-Based Metal−Organic Frameworks for the Detection and Removal of Antibiotics and Organic Explosives in Water. *J. Am. Chem. Soc.* **2016**, *138*, 6204.

(15) Weigel, L. F.; Nitsche, C.; Graf, D.; Bartenschlager, R.; Klein, C. D. Phenylalanine and Phenylglycine Analogues as Arginine Mimetics in Dengue Protease Inhibitors. *J. Med. Chem.* **2015**, *58*, 7719.

(16) For chiral COFs for HPLC separation, see: (a) Han, X.; Huang, J.; Yuan, C.; Liu, Y.; Cui, Y. Chiral 3D Covalent Organic Frameworks for High Performance Liquid Chromatographic Enantioseparation. *J. Am. Chem. Soc.* **2018**, *140*, 892. (b) Zhang, S.; Zheng, Y.; An, H.; Aguila, B.; Yang, C.-X.; Dong, Y.; Xie, W.; Cheng, P.; Zhang, Z.; Chen, Y.; Ma, S. Covalent Organic Frameworks with Chirality Enriched by Biomolecules for Efficient Chiral Separation. *Angew. Chem., Int. Ed.* **2018**, *57*, 16754. (c) Han, X.; Yuan, C.; Hou, B.; Liu, L.; Li, H.; Liu, Y.; Cui, Y. Chiral Covalent Organic Frameworks: Design, Synthesis and Property. *Chem. Soc. Rev.* **2020**, *49*, 6248.

(17) (a) Shinbo, T.; Yamaguchi, T.; Nishimura, K.; Sugiura, M. Chromatographic separation of racemic amino acids by use of chiral crown ether-coated reversed-phase packings. *J. Chromatogr.* **1987**, *405*, 145. (b) Hyun, M. H.; Jin, J. S.; Lee, W. Liquid chromatographic resolution of racemic amino acids and their derivatives on a new chiral stationary phase based on crown ether. *J. Chromatogr. A* **1998**, *822*, 155. (c) Berthod, A.; Liu, Y.; Bagwill, C.; Armstrong, D. W. Facile Liquid Chromatographic Enantioresolution of Native Amino Acids and Peptides Using a Teicoplanin Chiral Stationary Phase. *J. Chromatogr. A* **1996**, *731*, 123.

(18) (a) Kent, C. N.; Park, C.; Lindsley, C. W. Classics in Chemical Neuroscience: Baclofen. *ACS Chem. Neurosci.* **2020**, *11*, 1740. (b) Brown, K. M.; Roy, K. K.; Hockerman, G. H.; Doerksen, R. J.; Colby, D. A. Activation of the γ-Aminobutyric Acid Type B ($GABA_B$) Receptor by Agonists and Positive Allosteric Modulators. *J. Med. Chem.* **2015**, *58*, 6336.

https://dx.doi.org/10.1021/jacs.0c11276
J. Am. Chem. Soc. XXXX, XXX, XXX−XXX